Selective resonant radiation in quadratic crystals via group-velocity dispersion

Lili Bu [1,2,*] Gangzhou Wu [3] Shihua Chen [3,4] Stefano Trillo [5,†] and Fabio Baronio [2,‡]

[1] *School of Physics and Electronic Electrical Engineering, Huaiyin Normal University, 111 West Chang Jiang Road, 223300 Huaian, China*

[2] *Department of Information Engineering, University of Brescia, Via Branze 38, 25123 Brescia, Italy*

[3] *School of Physics and Frontiers Science Center for Mobile Information Communication and Security, Southeast University, Nanjing 211189, China*

[4] *Purple Mountain Laboratories, Nanjing 211111, China*

[5] *Department of Engineering, University of Ferrara, Via Saragat 1, 44122 Ferrara, Italy*

(Received 21 December 2025; accepted 26 February 2026; published 23 March 2026)

We consider the phenomenon of resonant radiation emitted by solitonlike wave packets in quadratic crystals and demonstrate the key role of the group-velocity dispersions, at the fundamental frequency and second harmonic, respectively, without any contribution from higher-order dispersions. In particular our approach allows us to predict a mechanism of primary resonance around the fundamental frequency component. Our theoretically predicted resonances are found to be in excellent agreement with numerical simulation of the propagation in a wide range of parameter values.

DOI: 10.1103/bh3y-8tqg

I. INTRODUCTION

Nonlinear waves spontaneously emit resonant radiation (RR), or Cherenkov radiation, when they become phase-matched to linear dispersive waves. In cubic media, as first recognized for silica fibers [1,2], phase-matching can be realized close to the zero of the group-velocity dispersion (GVD) due to the fundamental contributions of higher-order dispersions. The RR emission finds its importance mainly in photonic crystal fiber applications, serving as a tunable source of coherent radiation extending into the deep ultraviolet [3] and as a mechanism for spectral broadening in supercontinuum generation [4]. Similarly RR takes place in various platforms, including soliton-driven microcombs [5,6], line-defect waveguides [7], and chip-based waveguides pumped under normal GVD conditions [8]. RR phenomena also arise in contexts involving four-wave mixing processes [9], shock waves [10], and rogue waves [11].

RR has also been predicted in quadratic media [12–14] and experimentally demonstrated in bulk crystals such as β-barium borate (BBO) [15–17] or periodically poled lithium niobate [18]. Such results have been interpreted by considering the third-order dispersion or the full dispersion relationship (i.e., all higher-order dispersions), overlooking the role of GVDs. Recent studies have, however, highlighted the possibility that RR of solitons in second-harmonic generation (SHG) can arise solely from GVD (i.e., with no higher-order dispersion) both in the cascading limit [19,20] or under perfect phase-matching [21], a mechanism that can also be exploited in microresonators [22,23]. This is due to a pivotal role played by the second-harmonic (SH) component which drives, through its GVD, the resonance mechanism with linear dispersive waves, whereas dispersive components around the fundamental frequency (FF) can be generated through secondary processes of down-conversion [19–21].

In this article, our aim is to show that RR in SHG can arise, under proper regimes, also from a primary resonance around the FF. To this end, we develop resonance conditions that include the contribution from a possible small deviation from exact soliton excitation. We show that, depending specifically on the values of the GVDs, such conditions give rise to primary emission emerging around one of the two harmonic waves (FF or SH) or coexisting primary RRs around both.

II. THEORETICAL FRAMEWORK AND RR RELATIONS

We start from the dimensionless coupled equations obeyed by temporal envelopes u_1 at FF ω_0 and u_2 at SH $2\omega_0$ in dispersive quadratic media [19,24]:

$$iu_{1\xi} - \frac{\beta_1}{2}u_{1\tau\tau} + u_2 u_1^* e^{-i\delta k\xi} = 0,$$
$$iu_{2\xi} + ivu_{2\tau} - \frac{\beta_2}{2}u_{2\tau\tau} + u_1^2 e^{i\delta k\xi} = 0, \tag{1}$$

where $\xi = z/z_d = z|\beta_1''|/t_0^2$ is the normalized propagation distance, with $z_d = t_0^2/|\beta_1''|$ being the dispersion length, and $\beta_1 = \mathrm{sgn}(\beta_1'')$, $\beta_2 = \beta_2''/|\beta_1''|$, and $\beta_{1,2}'' = d^2k/d\omega^2|_{\omega_0,2\omega_0}$ are the GVDs. Here $\tau = (t - z/v_1)/t_0$ stands for time in a reference frame traveling with the FF group velocity v_1, and $v = z_d/z_w$ is the ratio between the dispersion length and the temporal walk-off length $z_w = t_0/(v_2^{-1} - v_1^{-1})$, where $v_{1,2} = dk/d\omega|^{-1}_{\omega_0,2\omega_0}$ are the (FF, SH) group velocities, and t_0 is a characteristic pulse temporal scale. $\delta k = \Delta k z_d$ is the

*Contact author: lili.bu@hytc.edu.cn
†Contact author: trlsfn@unife.it
‡Contact author: fabio.baronio@unibs.it

normalized wave number mismatch, with $\Delta k = 2k_1 - k_2$ and $k_{1,2} = k|_{\omega_0,2\omega_0}$. Moreover, $u_{1,2} = \chi z_d A_{1,2}$ where $|A_{1,2}|^2$ measure the intensities (W/m^2) with $\chi = \omega_0[2/(c^3\epsilon_0 n^2_{\omega_0} n_{2\omega_0})]^{1/2} d^{(2)}$, and $d^{(2)}$ is the nonlinear element (m/V). We look for the dynamics of Eqs. (1) in the forms

$$u_1 = s_1 + p_1, \; u_2 = s_2 + p_2, \tag{2}$$

where $s_{1,2}$ are the components of a two-color solitonlike solution of Eqs. (1), and $p_{1,2}$, with $|p_{1,2}| \ll |s_{1,2}|$, are the superposition of all the potential linear dispersive waves at both FF and SH in the systems. By inserting the ansatz (2) in Eq. (1), and neglecting quadratic terms in $p_{1,2}$, one can obtain that the complex perturbations $p_{1,2}$ obey the linearized equations:

$$\begin{aligned} ip_{1\xi} - \frac{\beta_1}{2} p_{1\tau\tau} &= -s_2 p_1^* e^{-i\delta k\xi} - s_1^* p_2 e^{-i\delta k\xi}, \\ ip_{2\xi} + iv p_{2\tau} - \frac{\beta_2}{2} p_{2\tau\tau} &= -2s_1 p_1 e^{i\delta k\xi}. \end{aligned} \tag{3}$$

Then we assume that $p_{1,2}$ consist of two parts

$$p_{1,2} = w_{1,2} + \psi_{1,2}, \tag{4}$$

where the terms $w_{1,2}$ account for perturbations at the same frequency of the soliton components $s_{1,2}$ that coexist with it (this is the typical situation in experiments, where the input pulses usually slightly differ from the exact soliton solution). The terms $\psi_{1,2}$ account instead for the RR induced by quadratic nonlinear waves, and hence behave like $\psi_{1,2} \sim e^{i(k_{1,2}\xi - \omega_{1,2}\tau_{nl})}$, with $\tau_{nl} = \tau - v_{nl}\xi$ being the retarded time in the soliton frame traveling with generic velocity v_{nl} [10], $\omega_{1,2}$ being the RR detuning frequencies, $k_1 = \beta_1\omega_1^2/2 - \omega_1 v_{nl}$, and $k_2 = \beta_2\omega_2^2/2 - \omega_2(v_{nl} - v)$.

To find the wave-number matching conditions of the generated RR waves, we assume that the nonlinear components s_1 and s_2 and potential perturbations w_1 and w_2 are fixed and constant sources of energy. As we see below, this assumption allows us to make excellent quantitative predictions of the frequencies of the generated waves. Substituting the ansatz (4) into Eqs. (3), we find that

$$\begin{aligned} i\psi_{1\xi} - \frac{\beta_1}{2}\psi_{1\tau\tau} + s_2\psi_1^* e^{-i\delta k\xi} + s_1^*\psi_2 e^{-i\delta k\xi} \\ = -s_1^* w_2 e^{-i\delta k\xi} - s_2 w_1^* e^{-i\delta k\xi}, \end{aligned} \tag{5}$$

$$i\psi_{2\xi} + iv\psi_{2\tau} - \frac{\beta_2}{2}\psi_{2\tau\tau} + 2s_1\psi_1 e^{i\delta k\xi} = -2s_1 w_1 e^{i\delta k\xi}. \tag{6}$$

The right-hand side (RHS) of Eq. (5) consists of two parts serving as driving sources for the wave ψ_1 at the FF. They originate from the mixing of the nonlinear component s_2 and wave w_1, and the nonlinear component s_1 and wave w_2. The RHS of Eq. (6) serves as a driving force for the wave ψ_2, at the SH, and depends on the mixing of the nonlinear component s_1 and wave w_1. For Eqs. (5) and (6) to have dispersive RR wave solutions, the operators on the left-hand side (LHS) should have continuum modes that can be excited by the RHS. To find the frequencies of these continuum modes, we neglect soliton-RR mixing due to $s\psi$ products in the LHS. At the FF, wave-number matching with the two driving terms in the RHS of Eq. (5) provides

$$\frac{\beta_1\omega_1^2}{2} - v_{nl}\omega_1 = -\delta k + k_{s_1}^*, \tag{7a}$$

$$\frac{\beta_1\omega_1^2}{2} - v_{nl}\omega_1 = -\delta k + k_{s_2}. \tag{7b}$$

Here k_{s_1,s_2} are the nonlinear wave numbers of $s_{1,2}$ components. Real solutions $\omega_1 = \omega_{1\mathrm{RR}}$ of Eqs. (7a) and (7b) yield RR frequency detuning with respect to FF central frequency. Similarly, wave-number matching with the driving term in the RHS of Eq. (6) provides

$$\frac{\beta_2\omega_2^2}{2} + (v - v_{nl})\omega_2 = \delta k + k_{s_1}, \tag{8}$$

with real solutions $\omega_2 = \omega_{2\mathrm{RR}}$ giving the RR detuning from SH central frequency.

III. BRIGHT SOLITON SOLUTIONS AND RR EMISSION

In the following, we focus on the case of anomalous GVD at FF and show that Eqs. (7a) and (8) are effective to predict resonance individually at FF or SH or both, depending on the relative value of GVDs, in particular, with zero or normal GVD at SH. First, we highlight the possibility of radiating exclusively through the GVD at FF. For this purpose, we consider a two-color bright soliton solution of Eqs. (1) [21], with $s_1(\tau,\xi) = \mathrm{sech}(\sqrt{-\gamma/\beta_1}\tau)e^{i\gamma\xi/2}$, $s_2(\tau,\xi) = \gamma s_1^2 e^{i\delta k\xi}$, $\beta_1 < 0$, $\beta_2 = 0$, $v = 0$, $v_{nl} = 0$, and $\gamma = [-\delta k + \sqrt{4 + \delta k^2}]/2$. In this case, Eq. (7a) gives real solutions $\omega^{\pm}_{1\mathrm{RR}} = \pm\sqrt{-(2\delta k + \gamma)/\beta_1}$, whereas neither Eq. (7b) nor Eq. (8) yields real solutions.

We have tested the predictions by integrating numerically Eqs. (1), considering such a two-color soliton at input, with $\beta_1 = -1$, $\beta_2 = 0$, $v = 0$, and mismatch $\delta k = 4$. The initial soliton condition is perturbed by coexisting small perturbations of the same shape, i.e., $w_{1,2} = 0.1 s_{1,2}$, equivalent to launching $u_{1,2}(\xi = 0, \tau) = 1.1 s_{1,2}(\xi = 0, \tau)$. Figures 1(a) and 1(b) report the resulting spatiotemporal evolutions, characterized by a weak RR emission at the FF. Figures 1(c) and 1(d) show the evolution and the input and output spectral FF and SH components, where the RR emerges as symmetric peaks in the FF spectrum that agree well with the expected frequency $\omega^{\pm}_{1\mathrm{RR}} = \pm 2.91$ from Eq. (7a). Such agreement is maintained in a wide range of mismatch values as reported in Fig. 1(e), where we compare the spectral peak from the numerics with those predicted from Eq. (7a). The SH spectrum in Fig. 1(d) does not show any primary RR, only peaks originating from frequency doubling of $\omega^{\pm}_{1\mathrm{RR}}$ ($2\omega^{\pm}_{1\mathrm{RR}} = \pm 5.74$).

Next, we want to highlight the possibility to radiate through the GVDs, individually around either FF or SH, or around both FF and SH, respectively. For this purpose, we consider the case of a two-color quadratic cascading bright solitary wave of Eqs. (1), $u_1 = \sqrt{2}\,\mathrm{sech}(\sqrt{2/\delta k}\tau)e^{i\xi/\delta k}$ and $u_2 = u_1^2 e^{i\delta k\xi}/\delta k$, with $\beta_1 = -1$, $v = 0$, and $\delta k > 0$. We summarize in Fig. 2 the expected RR frequencies, for this case. Figure 2(a) shows, as a function of mismatch δk, the branch $\omega^{+}_{1\mathrm{RR}}$ of the two symmetric peaks $\omega^{\pm}_{1\mathrm{RR}} = \pm\sqrt{-2(\delta k + 1/\delta k)/\beta_1}$ expected (regardless of the GVD ratio β_2) from Eq. (7a). Conversely no RR is expected from Eq. (7b) since its roots

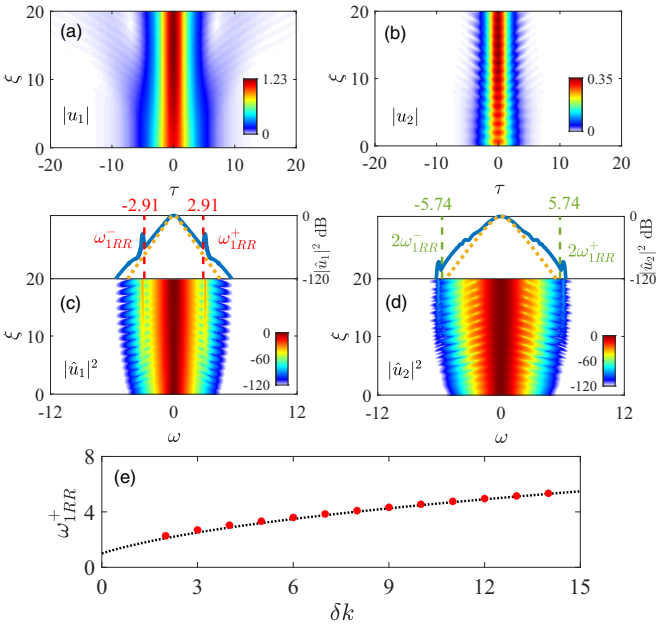

FIG. 1. Two-color soliton emitting RR at FF ($\beta_1 = -1$, $v = 0$, $\beta_2 = 0$, $\delta k = 4$). (a), (b) Spatiotemporal evolution of FF (a) and SH (b). (c), (d) spectral evolutions of FF (c) and SH (d), with the top boxes giving the spectral input (dashed yellow) and output (solid blue) profiles. In panel (c), the dashed lines labeled by $\omega^{\pm}_{1RR} = \pm 2.91$ stand for the RR frequencies from Eq. (7a). (e) RR peaks ω^{+}_{1RR} vs mismatch δk: numerical simulations (red dots) compared with predictions (dotted black) from Eq. (7a).

$\omega^{\pm}_{1RR} = \pm\sqrt{4/\delta k\beta_1}$ are imaginary. The positive branch of the symmetric peaks around SH at $\omega^{\pm}_{2RR} = \pm\sqrt{2(\delta k + 1/\delta k)/\beta_2}$ from Eq. (8) are shown in Fig. 2(b) against the GVD ratio β_2, for different mismatches δk. In Fig. 2 we outline three pilot examples, A, B, and C, which exhibit qualitatively different RR pictures, discussing below the outcome of the numerical integration of Eqs. (1) when launching the soliton perturbed by a small (linear) wave of the same shape.

Figure 3 is relative to case A in Fig. 2, i.e., $\beta_1 = -1$, $v = 0$, $\beta_2 = 0.05$, $\delta k = 6$, and input perturbations $w_{1,2} = 0.1 s_{1,2}$ [i.e., $u_{1,2}(\xi = 0, \tau) = 1.1 s_{1,2}(\xi = 0, \tau)$]. The temporal evolutions of the perturbed soliton in Figs. 3(a) and 3(b) display the emission of RR driven by FF, from both the leading and the trailing edges. Two distinct and symmetric spectral peaks

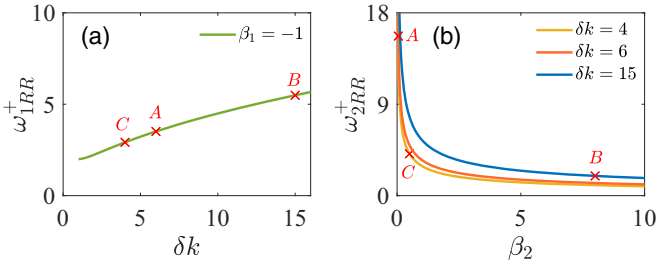

FIG. 2. Dependence of RR frequencies on the system parameters: (a) RR ω^{+}_{1RR} versus the effective mismatch δk, at fixed $\beta_1 = -1$, from Eq. (7a); (7b) RR frequency ω^{+}_{2RR} versus the GVD ratio β_2, at different mismatch δk, from Eq. (8).

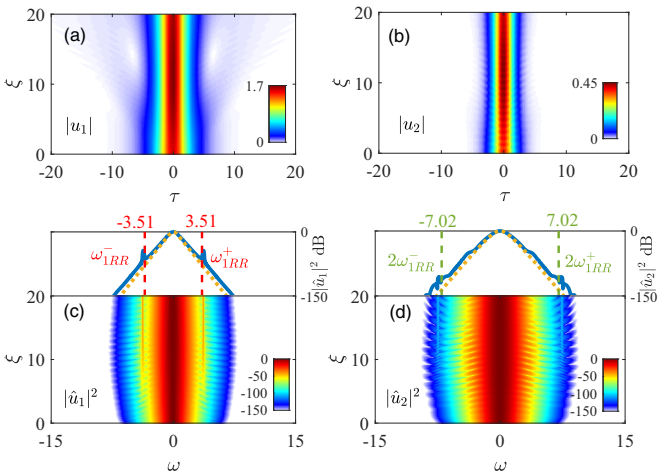

FIG. 3. RR emission from a cascading soliton at $\beta_1 = -1$, $v = 0$, $\beta_2 = 0.05$, and $\delta k = 6$ (case A in Fig. 2). (a), (b) Numerical temporal quadratic solitary wave evolution. (c), (d) The corresponding spatiospectral evolutions, with the top boxes giving the spectral input (dashed yellow) and output (solid blue) profiles, and analytical prediction for $\omega^{\pm}_{1RR}$ (red dashed vertical lines).

appear in the output spectral profile of the FF wave in Fig. 3(c), in agreement with the expected value $\omega^{\pm}_{1RR} = \pm 3.51$ from Eq. (7a). Importantly, the SH spectrum in Fig. 3(d) shows only evidence of secondary doubling of $\omega^{\pm}_{1RR}$ (i.e., peaks at $2\omega^{\pm}_{1RR} = \pm 7.02$), whereas the primary peaks expected at $\omega^{\pm}_{2RR} = \pm 17$ [see Fig. 2(b)] are too far detuned to be effectively seeded.

Figure 4 reports the case of a cascading soliton perturbed by $w_{1,2} = 0.05 s_{1,2}$ at $\beta_1 = -1$, $v = 0$, $\beta_2 = 8$, $\delta k = 15$ (case B in Fig. 2). In this case, a significant emission of RR occurs at the SH, from both the leading and trailing edges, as shown in Figs. 4(a) and 4(b). This corresponds to symmetric spectral peaks in Fig. 4(d) which agree with the prediction $\omega^{\pm}_{2RR} = \pm 1.94$ from Eq. (8). Contrary to case A in Fig. 3, RR at the FF

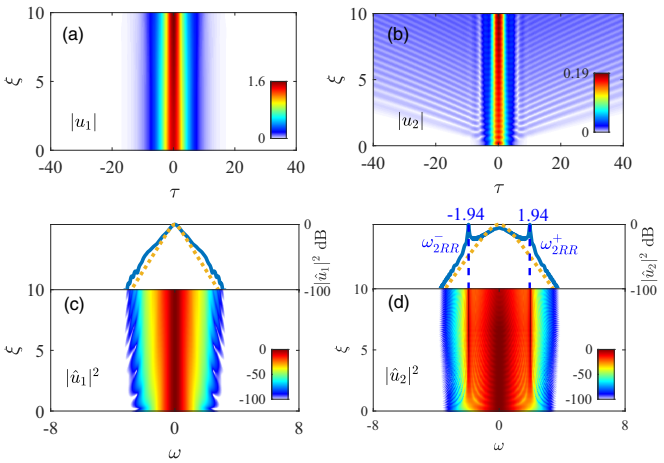

FIG. 4. As in Fig. 3 ($\beta_1 = -1$, $v = 0$), though with large SH-GVD $\beta_2 = 8$ and mismatch $\delta k = 15$ (case B in Fig. 2). The vertical dashed blue lines in the output SH spectrum stand for the prediction $\omega^{\pm}_{2RR}$ from Eq. (8).

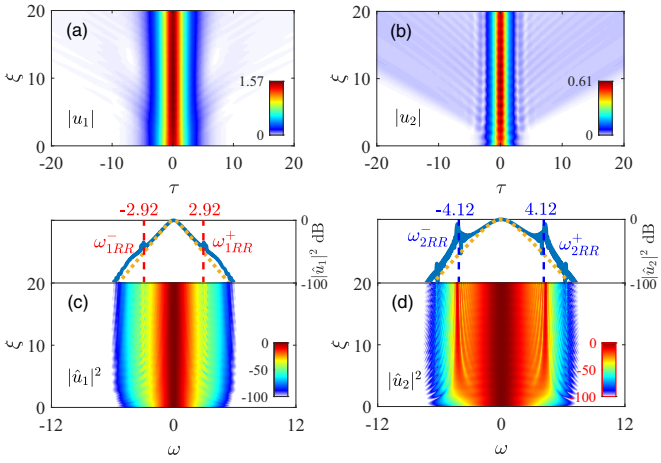

FIG. 5. As in Fig. 3 ($\beta_1 = -1$, $v = 0$), though with $\beta_2 = 1/2$ and $\delta k = 4$ (case C in Fig. 2). The red (blue) dashed lines in the output spectra stand for ω_{1RR} (ω_{2RR}) from Eq. 7(a) [Eq. (8)].

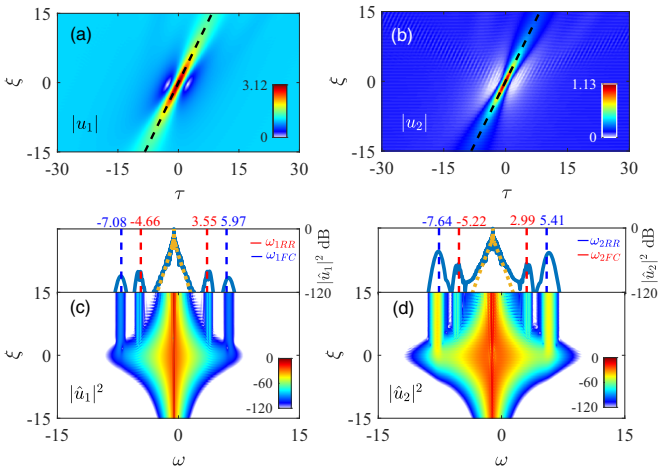

FIG. 6. As in Fig. 3 for a walking Peregrine soliton with parameters $\beta_1 = -1$, $\beta_2 = 0.4$, $v = 1$, and $\delta k = 8$. The red (blue) dashed lines in the output FF (SH) spectra stand for asymmetric $\omega^{\pm}_{1RR}$ ($\omega^{\pm}_{2RR}$) from Eq. (7a) [Eq. (8)]. The remaining dashed lines labeled $\omega^{\pm}_{1FC}$ and $\omega^{\pm}_{2FC}$ stand for peaks associated with secondary mixing processes (see text).

expected at $\omega^{\pm}_{1RR} = \pm 5.5$ is not effectively seeded and does not grow [see Fig. 4(c)].

Furthermore, we demonstrate the coexistence of RR generation at FF and at SH (case C in Fig. 2) by exciting again a perturbed cascading soliton with $w_{1,2} = 0.05 s_{1,2}$. Figures 5(a) and 5(b), obtained with $\beta_1 = -1$, $v = 0$, $\beta_2 = 0.5$, and $\delta k = 4$, show that the temporal evolution of the solitons is characterized by the emission of RR, from both the leading and the trailing edges, driven by FF and SH. Indeed two distinct and symmetric spectral peaks appear in the output spectral profile of the FF wave, which agree with the prediction $\omega^{\pm}_{1RR} = \pm 2.92$ from Eq. (7a), whereas two other incommensurate symmetric spectral peaks appear in the SH spectrum, in agreement with the prediction $\omega^{\pm}_{2RR} = \pm 4.12$ from Eq. (8).

In addition to exact solitons or approximated (cascading) solitary wave solutions of the bright type, Eqs. (1) admit similar solutions of the dark type [20,21,24]. We point out that the resonance conditions in Eqs. (7) and (8) provide a valid tool to predict the emergence of RR around the FF and/or the SH of dark solutions, similarly to the bright cases reported above and to the case explicitly discussed in Ref. [21] for dark solitons.

IV. WALKING PEREGRINE SOLITONS AND RR EMISSION

Finally, we show that the coexistence of RRs shown in Fig. 5 holds also for different situations such as a walking Peregrine soliton propagating under anomalous-normal GVDs at FF-SH, respectively [19]. In this case, we explicitly account for the group-velocity mismatch between the FF and the SH ($v \neq 0$). The walking Peregrine soliton can be written as $s_1(\xi,\tau) = [1 - \frac{2i\gamma\xi+1}{\gamma\theta^2+\gamma^2\xi^2+1/4}]\exp[i(K\xi - \Omega\theta)]$ and $s_2(\xi,\tau) = \gamma u_1^2 e^{i\delta k\xi}$, where $K = \gamma - v_p^2/2\beta_1$, $\Omega = v_p/\beta_1$, $\theta = \tau - v_p\xi$, $v_{nl} \equiv v_p = v\beta_1/(\beta_1 - 2\beta_2)$ is the soliton velocity, and $\gamma = \frac{vv_p - \beta_1\delta k - \sqrt{8\beta_1^2 + (vv_p - \beta_1\delta k)^2}}{4\beta_1}$ (see Ref. [21] for details). In this case, we expect primary resonances around the FF at $\omega^{\pm}_{1RR} = [v_p \pm \sqrt{-2\beta_1(\delta k + \gamma) + 2v_p^2}]/\beta_1$ from Eq. (7a) and around the SH at $\omega^{\pm}_{2RR} = [v_p - v \pm \sqrt{2\beta_2(\delta k + \gamma) + (v_p - v)^2 - v_p^2\beta_2/\beta_1}]/\beta_2$ from Eq. (8), whereas, again, Eq. (7b) does not give real solutions. We have tested the predictions by integrating numerically Eqs. (1) with launching conditions $u_{1,2}(\xi = 0, \tau) = 1.05 s_{1,2}(\xi = 0, \tau)$, i.e., a two-color Peregrine soliton perturbed by terms $w_{1,2} = 0.05\ s_{1,2}$. An example for $\beta_1 = -1$, $v = 1$, $\beta_2 = 0.4$, and $\delta k = 8$ is displayed in Fig. 6. The temporal evolutions in Figs. 6(a) and 6(b) clearly show that the FF and SH components travel with locked velocity $v_p = 5/9$ (black dashed lines). The spectra in Figs. 6(c) and 6(d) show that the central frequencies of the FF and SH components are red-shifted by $\Omega = v_p/\beta_1$ and $2\Omega = 2v_p/\beta_1$, respectively. The generated RR spectral peaks are symmetrically located with respect to such central frequencies (Ω at FF, 2Ω at SH). The peaks in the numerical spectra agree well with the prediction of RR frequencies that yield $\omega^-_{1RR} = -4.66$ and $\omega^+_{1RR} = 3.55$ [red dashed lines in Fig. 6(c)], and $\omega^-_{2RR} = -7.64$ and $\omega^+_{2RR} = 5.41$ [blue dashed lines in Fig. 6(d)]. Additionally, other spectral peaks are visible, due to secondary frequency conversion processes. In Fig. 6(d) the mixing $\Omega + \omega^{\pm}_{1RR} = \omega^{\pm}_{2FC}$ [corresponding to real-world sum frequency generation $(\omega_0 + \Omega/t_0) + (\omega_0 + \omega^{\pm}_{1RR}/t_0) = 2\omega_0 + (\Omega + \omega^{\pm}_{1RR})/t_0$] gives additional peaks $\omega^-_{2FC} = -5.22$ and $\omega^+_{2FC} = 2.99$. Similarly, the mixing $\omega^{\pm}_{2RR} - \Omega = \omega^{\pm}_{2FC}$ [corresponding to real-world difference frequency generation $(2\omega_0 + \omega^{\pm}_{2RR}/t_0) - (\omega_0 + \Omega/t_0) = \omega_0 + (\omega^{\pm}_{2RR} - \Omega)/t_0$] gives the peaks $\omega^-_{1FC} = -7.08$ and $\omega^+_{1FC} = 5.97$ in Fig. 6(c).

V. CONCLUSION

In summary, we have shown that perturbed quadratic solitons can resonantly radiate linear dispersive waves thanks to phase matching relying solely on GVDs at FF and SH without contributions from higher-order dispersion. The main interest here, with respect to previous works [19–21], is the extension to conditions with a primary resonance around the FF.

Depending on the values of the GVDs and mismatch, primary emission can occur around one of the harmonics (FF or SH), or coexist around both harmonics. We remark that our study considers the dimensionless model and quantities identifying different regimes of RR emission in quadratic crystals and within these different regimes many real experiments can be realized in BBO, $LiNbO_3$, and KTP crystals.

Finally, we emphasize that, while Eqs. (7) and (8) give accurate predictions of RR, as a matter of fact, in all cases shown, good estimates of such RR frequencies can be obtained by neglecting the soliton parameters (velocity and nonlinear shift), thus approximating Eqs. (7) as $\beta_1\omega_1^2/2 = -\delta k$ and Eq. (8) as $\beta_2\omega_2^2/2 + v\omega_2 = \delta k$, which can be effectively used as a rule of thumb in most experiments.

ACKNOWLEDGMENTS

This work was supported by Progetti di Ricerca di Interesse Nazionale (PRIN) funded by the European Union–Next Generation EU, Mission 4, Component C2 (Project No. 20222NCTCY), and by the National Natural Science Foundation of China (Project No. 12374301).

DATA AVAILABILITY

The data that support the findings of this article are not publicly available. The data are available from the authors upon reasonable request.

[1] P. K. A. Wai, C. R. Menyuk, Y. C. Lee, and H. H. Chen, Nonlinear pulse propagation in the neighborhood of the zero-dispersion wavelength of monomode optical fibers, Opt. Lett. **11**, 464 (1986).

[2] N. Akhmediev and M. Karlsson, Cherenkov radiation emitted by solitons in optical fibers, Phys. Rev. A **51**, 2602 (1995).

[3] X. Liu, A. S. Svane, J. Lægsgaard, H. Tu, S. A. Boppart, and D. Turchinovich, Progress in Cherenkov femtosecond fiber lasers, J. Phys. D: Appl. Phys. **49**, 023001 (2016).

[4] D. V. Skryabin and A. V. Gorbach, *Colloquium*: Looking at a soliton through the prism of optical supercontinuum, Rev. Mod. Phys. **82**, 1287 (2010).

[5] V. Brasch, M. Geiselmann, T. Herr, G. Lihachev, M. H. P. Pfeiffer, M. L. Gorodetsky, and T. J. Kippenberg, Photonic chip-based optical frequency comb using soliton Cherenkov radiation, Science **351**, 357 (2016).

[6] X. Yi, Q.-F. Yang, X. Zhang, K. Y. Yang, X. Li, and K. Vahala, Single-mode dispersive waves and soliton microcomb dynamics, Nat. Commun. **8**, 14869 (2017).

[7] P. Colman, S. Combrié, G. Lehoucq, A. de Rossi, and S. Trillo, Blue self-frequency shift of slow solitons and radiation locking in a line-defect waveguide, Phys. Rev. Lett. **109**, 093901 (2012).

[8] Y. Okawachi, M. Yu, J. Cardenas, X. Ji, M. Lipson, and A. L. Gaeta, Coherent, directional supercontinuum generation, Opt. Lett. **42**, 4466 (2017).

[9] M. Erkintalo, Y. Q. Xu, S. G. Murdoch, J. M. Dudley, and G. Genty, Cascaded phase matching and nonlinear symmetry breaking in fiber frequency combs, Phys. Rev. Lett. **109**, 223904 (2012).

[10] M. Conforti, F. Baronio, and S. Trillo, Resonant radiation shed by dispersive shock waves, Phys. Rev. A **89**, 013807 (2014).

[11] F. Baronio, S. Chen, and S. Trillo, Resonant radiation from Peregrine solitons, Opt. Lett. **45**, 427 (2020).

[12] M. Bache, O. Bang, B. B. Zhou, J. Moses, and F. W. Wise, Optical Cherenkov radiation in ultrafast cascaded second-harmonic generation, Phys. Rev. A **82**, 063806 (2010).

[13] B. B. Zhou, A. Chong, F. W. Wise, and M. Bache, Ultrafast and octave-spanning optical nonlinearities from strongly phase-mismatched quadratic interactions, Phys. Rev. Lett. **109**, 043902 (2012).

[14] W. R. Rowe, D. V. Skryabin, and A. V. Gorbach, Temporal quadratic solitons and their interaction with dispersive waves in lithium niobate nanowaveguides, Phys. Rev. Res. **1**, 033146 (2019).

[15] B. Zhou, H. Guo, and M. Bache, Energetic mid-IR femtosecond pulse generation by self-defocusing soliton-induced dispersive waves in a bulk quadratic nonlinear crystal, Opt. Express **23**, 6924 (2015).

[16] B. Zhou and M. Bache, Dispersive waves induced by self-defocusing temporal solitons in a beta-barium-borate crystal, Opt. Lett. **40**, 4257 (2015).

[17] B. Zhou and M. Bache, Invited article: Multiple-octave spanning high-energy mid-IR supercontinuum generation in bulk quadratic nonlinear crystals, APL Photonics **1**, 050802 (2016).

[18] B. B. Zhou, X. Liu, H. R. Guo, X. L. Zeng, X. F. Chen, H. P. Chung, Y. H. Chen, and M. Bache, Parametrically tunable soliton-induced resonant radiation by three-wave mixing, Phys. Rev. Lett. **118**, 143901 (2017).

[19] L. Bu, F. Baronio, S. Chen, and S. Trillo, Quadratic Peregrine solitons resonantly radiating without higher-order dispersion, Opt. Lett. **47**, 2370 (2022).

[20] L. Bu, S. Chen, F. Baronio, and S. Trillo, Resonant radiation emitted by solitary waves via cascading in quadratic media, Opt. Express **31**, 8307 (2023).

[21] L. Bu, G. Wu, C. Hou, S. Chen, P. Grelu, and F. Baronio, Soliton resonant radiation in phase-matched second-harmonic generation, Phys. Rev. A **109**, 013510 (2024).

[22] G. Wu, C. Hou, Y. Wei, S. Chen, T. Lin, F. Baronio, and Z. Ni, Diverse interlocked switching waves in cavity-enhanced second-harmonic generation, Opt. Express **32**, 45436 (2024).

[23] G. Wu, Y. Wei, L. Li, S. Chen, L. Bu, F. Baronio, T. Lin, M. Zhu, S. Trillo, and Z. Ni, Ultraflat soliton microcombs in driven quadratic-Kerr nonlinear microresonators, Phys. Rev. Lett. **135**, 113801 (2025).

[24] A. V. Buryak, P. D. Trapani, D. V. Skryabin, and S. Trillo, Optical solitons due to quadratic nonlinearities: From basic physics to futuristic applications, Phys. Rep. **370**, 63 (2002).